A novel impact identification algorithm based on a linear approximation with maximum entropy

N. Sanchez, V. Meruane*, A. Ortiz-Bernardin

Department of Mechanical Engineering, Universidad de Chile, Beauchef 851, Santiago, Chile

E-mail: *vmeruane@ing.uchile.cl

Abstract. This article presents a novel impact identification algorithm that uses a linear approximation handled by a statistical inference model based on the maximum-entropy principle, termed linear approximation with maximum entropy (LME). Unlike other regression algorithms as Artificial Neural Networks (ANN) and Support Vector Machines (SVM), the proposed algorithm requires only parameter to be selected and the impact is identified after solving a convex optimization problem that has a unique solution. In addition, with LME data is processed in a period of time that is comparable to the one of other algorithms. The performance of the proposed methodology is validated by considering an experimental aluminum plate. Time varying strain data is measured using four piezoceramic sensors bonded to the plate. To demonstrate the potential of the proposed approach over existing ones, results obtained via LME are compared with those of ANN and Least Square Support Vector Machines (LSSVM). The results demonstrate that with a low number of sensors it is possible to accurately locate and quantify impacts on a structure and that LME outperforms other impact identification algorithms.

Keywords: Impact identification, structural health monitoring, damage assessment, maximum entropy, linear approximation.
Submitted to: *Smart Mater. Struct.*

1. Introduction

Detecting, locating and quantifying incipient damage on a structure generates a wide interest in the mechanical, aeronautical, aerospace and civil engineering fields. Structural damage assessment guarantees the integrity of the structure, which has a tremendous potential for life-safety and/or economic benefits. Damage due to an external impact is a concern in structural design. For example, aircraft are susceptible to impacts from collisions of birds, runway stones and tools dropped during maintenance. To avoid catastrophic failures it is of critical importance to detect the presence of an impact damage as soon as it occurs. However, this type of damage, known as Barely

Visible Impact Damage (BVID), is usually internal and there are no visible indications of its presence on the surface.

BVID can be detected by Non-Destructive Testing (NDT) techniques such as x-ray, c-scan or visual inspections. Nevertheless, these techniques are time-consuming, require access to the portion of the structure being inspected and can only be performed when the system is out of service, which can be impractical in some cases. Impact identification methodologies have been proposed as a complement to NDT. These methodologies would continuously monitor the structure, detecting, locating and quantifying impacts as they occur. For impact damage, its extend is correlated with the impact energy. Therefore, by locating and quantifying impacts over a structure it is feasible to predict possible damage locations, which allows to schedule inspections only when they are necessary and to perform a localized search, saving inspection time.

Impact identification methodologies can be divided into two groups: model-based [1, 2] and data-driven [3–13] algorithms. Model-based impact identification involves the solution of a nonlinear inverse problem that requires to evaluate the numerical model several times, which can be exceedingly slow for real-time applications. In addition, model-based algorithms rely on the precision of the numerical model, and any error in the numerical model will be interpreted as an impact identification error. Within data-driven algorithms, methodologies based on classification, pattern recognition and regression have been proposed, being Artificial Neural Networks (ANN) the most frequently used. Worden and Staszewski [3] and Staszewski et al. [14] used two feed-forward Multi-Layer Perceptron (MLP) networks to identify impacts on a composite plate. The first network was trained to detect the impact location, whereas the second network quantifies the impact magnitude. Haywood et al. [5] investigated two approaches to locate impacts in a composite panel with embedded piezoceramic sensors: MLP network and GA-based triangulation. They concluded that both approaches provide a similar degree of accuracy. LeClerc et al. [6] applied a two-step impact detection algorithm to an aircraft component. First, a classification network finds the region of the impact and afterwards another network localizes its position. With this methodology the researchers were able to obtain better results than those of a single neural network. Sharif-Khodaei et al. [8] trained a neural network to detect impacts location on a composite stiffened panel. The network was trained and tested with data obtained from a finite element model of the structure and the numerical model was validated with experimental data.

Although ANN can process data very quickly, the slow learning speed and the large number of parameters that need to be tuned within the training stage are drawbacks in their application. In the parametric study performed by Sharif-Khodaei et al. [8] it was demonstrated that the performance of a neural network for impact localization strongly depends on the network architecture (number of layers and number of hidden nodes) and network properties (transfer functions and training algorithm). In addition, ANN have the disadvantage of over-fitting and getting stuck in local minimum. An alternative are Support Vector Machines (SVM), which exhibit the advantage of global

optimization and higher generalization capabilities than ANN. Least Squares Support Vector Machines (LSSVM) further simplifies the regression to a problem that can be solved from a set of linear equations [15]. Xu [13] implemented a LSSVM to locate and quantify impacts in an aluminum plate and the results are compared with those of an ANN approach, demonstrating that LSSVM reaches more accurate results. Fu and Xu [9] proposed a two-layer SVM to predict the location of impacts on an aluminum plate structure. Input data is obtained from a Principal Component Analysis (PCA) of the strain time signal of piezoelectric sensors located over the plate. The results are compared with those of an ANN, concluding that SVM are capable of accomplishing better impact localization accuracy than ANN. To overcome the slow learning speed of ANN, Huang et al. [16] proposed a new learning algorithm called the extreme learning machine (ELM), which is suitable for single-layer feed-forward networks. This algorithm provides good generalization at fast learning speeds, and the only parameter that needs to be tuned is the number of hidden nodes. Since it was first introduced in 2004, the ELM algorithm has attracted the attention of increasing number of researchers [17]. Xu [12] compared the algorithm performance among a basic ELM, kernel-ELM and LSSVM to localize impacts in an aluminum plate. Xu concluded that kernel-ELM is as precise as LSSVM with lower training and evaluation times. Fu et al. [11] implemented a kernel-ELM for impact localization using PCA to extract features. Results in accuracy are similar to those of the SVM, but the kernel-ELM is faster, making it suitable for real-time applications. The time-reversal approach as been presented as a precise alternative for impact localization [18–21]. This a one-class nearest neighbor algorithm, in which the correlation between different impacts is measured by the signals convolution.

A new nonparametric method for supervised learning was presented by Gupta et al. [22, 23]. This method generalized linear approximation by using the maximum-entropy (max-ent) principle for statistical inference [24]. Meruane et al. [25, 26] demonstrated the applicability of the Linear Approximation with Maximum Entropy (LME) method in structural damage identification. They showed that LME achieves more accurate results than ANN at a similar evaluation speed. Herein, we demonstrate the applicability of LME to the impact identification problem.

The primary contribution of this research is the development of a novel impact identification algorithm that uses a linear approximation method. The linear approximation is handled by a statistical inference model based on the maximum-entropy principle [24]. The merits of this approach are threefold: only one parameter needs to be selected, the impact is identified after solving a convex optimization problem that has a unique solution and data is processed in a period of time that is comparable to the one of other regression algorithms such as ANN and SVM. In addition, LME does not require classical training in which the algorithm is trained once and then the training data is discarded, but performs a linear interpolation using the training data to estimate the impact. The main advantage is that new data can be easily incorporated to the training database with no need of re-training the algorithm as in the case of ANN and SVM. The performance of the proposed methodology is validated by considering an

experimental aluminum plate. To demonstrate the potential of the proposed approach over existing ones, results obtained via LME are compared with those of an ANN and a LSSVM [13].

In general, with an appropriate number of sensors distributed over the structure it is possible to accurately locate and quantify impacts. Nevertheless, the objective of an impact identification algorithm is to locate and quantify impacts with precision using the minimum number of sensors possible, thus minimizing the instrumentation cost and avoiding unnecessary wiring. Here, time varying strain data is measured using only four piezoceramic sensors bonded to the plate.

The remainder of this work is structured as follows: Section 2 presents the proposed impact identification methodology. Section 3 describes the experimental setup. Section 4 presents the impact identification results using three approaches: LME, ANN and LSSVM. Finally, conclusions and forthcoming work are presented in Section 5.

2. Impact identification methodology

2.1. Signal processing and feature extraction

The principle of an impact identification algorithm is to detect, locate and quantify an impact force, with the use of a passive system consisting of sensors distributed over the structure. Figure 1 illustrates a typical experimental setup for impact identification, where piezoelectric sensors bonded to the structure detect surface stress waves generated by the impact.

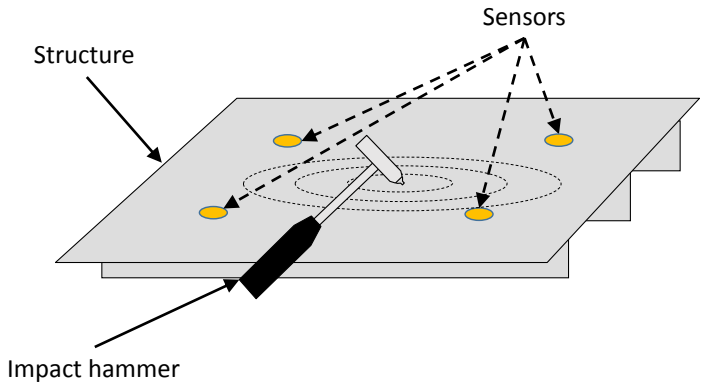

Figure 1. Scheme of an experimental setup for impact identification.

Figure 2 presents an example of a strain-time signal obtained from an impact test. It also shows the frequency spectrum computed from the Fourier transform and the signal envelope obtained through the Hilbert transform [27].

The amount of strain-time data collected by the sensors is too large to be used directly in a classification or regression algorithm. Therefore, preprocessing of the data is necessary to extract characteristics features. In the literature, different features

extracted from the signals in the time or frequency domain have been studied. Some example are [5]:

- Maximum and minimum signal amplitude.
- Times at maximum and minimum amplitude.
- Real and imaginary parts of each spectrum integrated over frequency.
- Maximum and minimum of signal envelope.
- Times at maximum and minimum of signal envelope.
- Times of beginning and end of signal envelope.

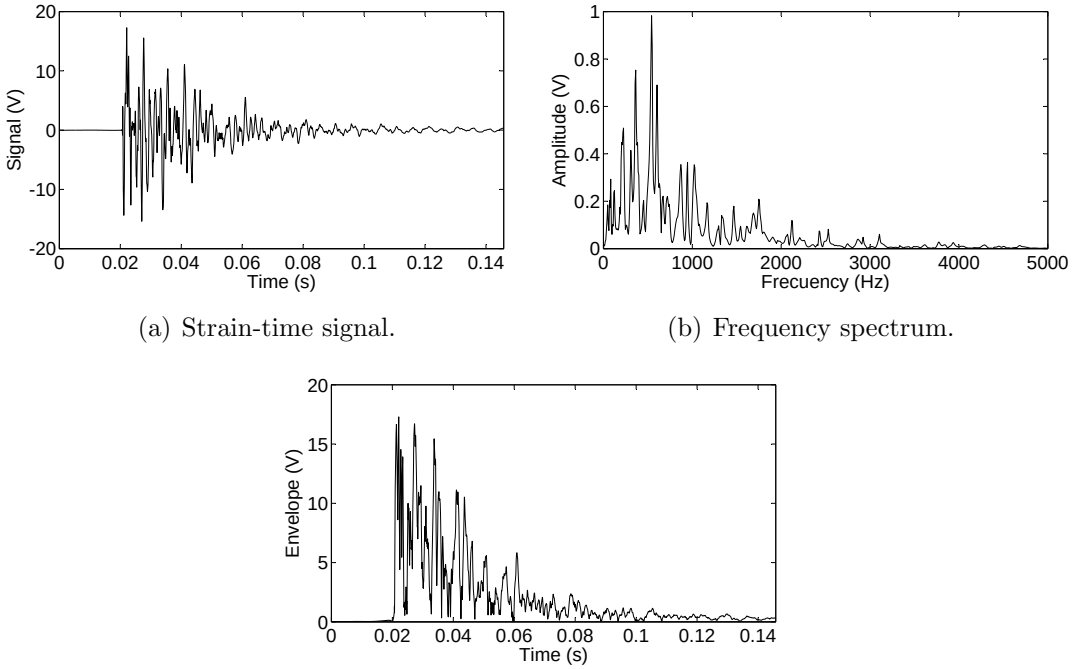

(a) Strain-time signal.

(b) Frequency spectrum.

(c) Signal envelope.

Figure 2. Example of a strain time signal along with its frequency spectrum and envelope.

Various studies have shown that the best features for impact identification are the time and magnitude of the maximum, and the time of arrival measured as the time the signal exceeds a certain threshold [3, 5, 8]. In the present investigation, after testing different combinations, it was concluded that the best results are obtained when the following features are used:

(i) **Maximum of signal envelope.**

(ii) **Time of arrival of signal envelope.** The threshold value was defined as a 10% of the maximum signal amplitude. This time is computed as the elapse time between the arrival of the first strain signal (among all sensors) and the arrival of the current signal.

(iii) **Time of the first peak.** Defined as the time of the first peak with an amplitude equal or higher than 50% the maximum of the signal envelope, a peak is defined as a local maxima in the signal envelope. This time is computed as the elapse time between the arrival of the first strain signal (among all sensors) and the time of the first peak in the current signal.

As an example, Figure 3 illustrates the identification of the time of the first peak and time of arrival in two different signals. The horizontal red line indicates 50% of the maximum amplitude in the signal, and a red cross shows the first peak that exceeds the threshold impose by the red line. The horizontal blue line indicates 10% of the maximum amplitude and a blue cross shows the first time the signal reaches this value. It should be noted that the time of arrival and the time of the first peak are defined relative to the time of the first strain signal, which depends on the sensors and impact location. An absolute reference would be the time of the impact or a fixed reference sensor, but in a real application the impact is not measured and the only information available is the signal given by the sensors. On the other hand, using always the same sensor as reference would result in negative arrival times.

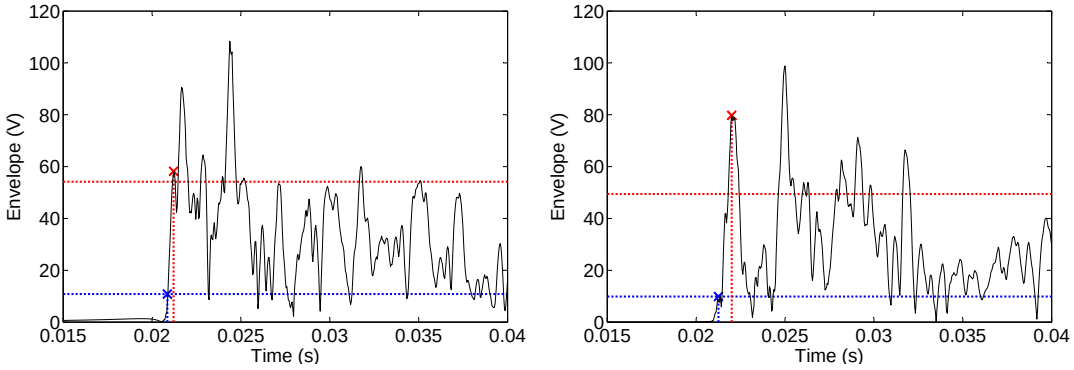

(a) Example 1 (b) Example 2

Figure 3. Identification of the first peak and time of arrival.

2.2. Linear approximation with maximum entropy

Let define the observation vector $\mathbf{Y}^j = \left\{Y_1^j, Y_2^j, Y_3^j\right\} \in \mathbb{R}^3$ representing the jth impact to a structure, where Y_1^j, Y_2^j are the x and y coordinates of the force location and Y_3^j is the force magnitude. Let the feature vector $\mathbf{X}^j = \left\{X_1^j, X_2^j, \ldots, X_n^j\right\} \in \mathbb{R}^n$ represent a set of characteristics response parameters associated to the impact $\mathbf{Y}^j$. In the present case, the structure has four piezoelectric sensors, and three features are extracted from the signal envelope of each sensor, as described in the previous section. Therefore, the feature vector $\mathbf{X}^j$ contains 12 parameters.

Assuming that a database with a set of N impact is constructed $(\mathbf{X}^1, \mathbf{Y}^1), (\mathbf{X}^2, \mathbf{Y}^2)$ $, \ldots, (\mathbf{X}^N, \mathbf{Y}^N)$, then the central problem in impact identification is: given a certain feature $\mathbf{X}$, estimate the corresponding impact $\mathbf{Y}$. The nearest neighbor regression

estimate of $\mathbf{Y}$ is given by

$$\hat{\mathbf{Y}} = \sum_{j=1}^{k} w_j(\mathbf{X})\mathbf{Y}^j, \tag{1}$$

where $\mathbf{Y}^1, \mathbf{Y}^2, \ldots, \mathbf{Y}^k$ are the observation vectors associated to the k closest neighbors to the test vector $\mathbf{X}$, and $w_1(\mathbf{X}), w_2(\mathbf{X}), \ldots, w_k(\mathbf{X})$ are weighting functions. The k nearest neighbor (k-NN) algorithm weights each neighbor equally, thus $w_i(\mathbf{X}) = 1/k$, for $i =$ 1 to k. Whereas, a kernel nearest neighbor algorithm base weightings on the distance from the test vector $\mathbf{X}$ to each vector in the database [28].

On the other hand, linear interpolation takes the N feature vectors in the database and uses a linear combination of them to represent $\mathbf{X}$ as [29]

$$\mathbf{X} = \sum_{j=1}^{N} w_j(\mathbf{X})\mathbf{X}^j, \quad \sum_{j=1}^{N} w_j(\mathbf{X}) = 1, \tag{2}$$

where $\mathbf{X}^1, \mathbf{X}^2, \ldots, \mathbf{X}^N$ are the feature vectors in the database set. Once the weighting functions are determined, then $\mathbf{Y}$ is estimated from (1) with $k = N$. Typically Equation (2) is undetermined, and its solution can be tackled via an unconstrained optimization technique of the family of least-squares. However, these methods produce some negative weights, which lacks physical meaning. An alternative that produces positive weights is obtained via the maximum-entropy (max-ent) variational principle [24].

The notion of entropy in information theory was introduced by Shannon as a measure of uncertainity [30]. Later on using the Shannon entropy, Jaynes [24] postulated the maximum-entropy principle as a rationale means for least-biased statistical inference when insufficient information is available. The maximum-entropy principle is suitable to find the least-biased probability distribution when there are fewer constraints than unknowns and is posed as follows:

Consider a set of N discrete events $\{x_1, \ldots, x_N\}$. The possibility of each event is $p_i = p(x_i) \in [0, 1]$ with uncertainty $-\ln p_i$. The Shannon entropy $H(\mathbf{p}) = -\sum_{i=1}^{N} p_i \ln p_i$ is the amount of uncertainty represented by the distribution $\{p_1, \ldots, p_N\}$. The least-biased probability distribution and the one that has the most likelihood to occur is obtained via the solution of the following optimization problem (maximum-entropy principle):

$$\max_{\mathbf{p}\in\mathbb{R}_+^N} \left[H(\mathbf{p}) = -\sum_{i=1}^{N} p_i \ln(p_i) \right], \tag{3a}$$

subject to the constraints:

$$\sum_{i=1}^{N} p_i = 1, \quad \sum_{i=1}^{N} p_i g_r(x_i) =< g_r(x) >, \tag{3b}$$

where $\mathbb{R}_+^N$ is the non-negative orthant and $< g_r(x) >$ is the known expected value of functions $g_r(x)$ $(r = 0, 1, \ldots, m)$, with $g_0(x) = 1$ being the normalizing condition.

The optimization problem (3) assigns probabilities to every x_i in the set. Now, assume that the probability p_i has an initial guess m_i known as a *prior*, which reduces its uncertainty to $-\ln p_i + \ln m_i = -\ln(p_i/m_i)$. An alternative problem can be formulated by using this *prior* in (2) [31]:

$$\max_{\mathbf{p}\in\mathbb{R}^n_+} \left[H(\mathbf{p}) = -\sum_{i=1}^{N} p_i \ln\left(\frac{p_i}{m_i}\right) \right], \tag{4a}$$

subject to the constraints:

$$\sum_{i=1}^{n} p_i = 1, \quad \sum_{i=1}^{n} p_i g_r(x_i) =< g_r(x) > . \tag{4b}$$

In (4), the variational principle associated with $\sum_{i=1}^{N} p_i \ln\left(\frac{p_i}{m_i}\right)$ is known as *the principle of minimum relative (cross) entropy* [32, 33]. Depending upon the *prior* employed, the optimization problem (4) will favor some x_i in the set by assigning more probability to them, and eventually, assigning non-zero probability ($p_i > 0$) to a selected number of x_i ($i < N$) in the set. It can be easily seen that if the *prior* is constant, the Shannon-Jaynes entropy functional (3) is recovered as a particular case.

Because of its general character and flexibility, we adopt the relative entropy approach for our problem, where the probability p_i and the discrete event x_i is replaced with the weighting function w_i and the feature vector $\mathbf{X}^i$ of the linear approximation problem posed in (2), respectively. This reads:

$$\max_{\mathbf{w}\in\mathbb{R}^N_+} \left[H(\mathbf{w}) = -\sum_{i=1}^{N} w_i(\mathbf{X}) \ln\left(\frac{w_i(\mathbf{X})}{m_i(\mathbf{X})}\right) \right], \tag{5a}$$

subject to the constraints:

$$\sum_{i=1}^{N} w_i(\mathbf{X})\tilde{\mathbf{X}}^i = 0, \quad \sum_{i=1}^{N} w_i(\mathbf{X}) = 1, \tag{5b}$$

where $\tilde{\mathbf{X}}^i = \mathbf{X}^i - \mathbf{X}$ has been introduced as a shifted measure for stability purposes. Different prior distributions can be used, typical ones are: Gaussian, cubic spline, quartic spline or constant [34]. Here we tested the four distributions and the best performance was obtained with a smooth Gaussian,

$$m_i(\mathbf{X}) = \exp(-\beta_i \|\tilde{\mathbf{X}}^i\|^2), \tag{6}$$

where $\beta_i = \gamma/h_i^2$; γ is a parameter that controls the support of the Gaussian prior at $\mathbf{X}^i$, and therefore its associated weight function; and h_i is a characteristic $n-$dimensional Euclidean distance between neighbors that can be distinct for each $\mathbf{X}^i$. In view of the optimization problem posed in (5) for supervised learning, maximizing the entropy chooses the weight solution that commits the least to any one in the database samples [23].

The solution of the max-ent optimization problem is handled by using the procedure of Lagrange multipliers, which yields [31]:

$$w_i(\mathbf{X}) = \frac{Z_i(\mathbf{X};\boldsymbol{\lambda}^*)}{Z(\mathbf{X};\boldsymbol{\lambda}^*)}, \quad Z_i(\mathbf{X};\boldsymbol{\lambda}^*) = m_i(\mathbf{X})\exp(-\boldsymbol{\lambda}^* \cdot \tilde{\mathbf{X}}^i), \tag{7}$$

where $Z(\mathbf{X};\boldsymbol{\lambda}^*) = \sum_j Z_j(\mathbf{X};\boldsymbol{\lambda}^*)$, $\tilde{\mathbf{X}}^i = [\tilde{X}_1^i \dots \tilde{X}_N^i]^{\mathrm{T}}$ and $\boldsymbol{\lambda}^* = [\lambda_1^* \dots \lambda_N^*]^{\mathrm{T}}$.

In (7), the Lagrange multiplier vector $\boldsymbol{\lambda}^*$ is the minimizer of the dual optimization problem posed in (5) [31]:

$$\boldsymbol{\lambda}^* = \arg\min_{\boldsymbol{\lambda}\in\mathbb{R}^N} \ln Z(\mathbf{X};\boldsymbol{\lambda}), \tag{8}$$

which gives rise to the following system of nonlinear equations:

$$\mathbf{f}(\boldsymbol{\lambda}) = \nabla_{\boldsymbol{\lambda}} \ln Z(\boldsymbol{\lambda}) = -\sum_i^N w_i(\mathbf{X})\tilde{\mathbf{X}}^i = \mathbf{0}, \tag{9}$$

where $\nabla_{\boldsymbol{\lambda}}$ stands for the gradient with respect to $\boldsymbol{\lambda}$. Once the converged $\boldsymbol{\lambda}^*$ is found, the weight functions are computed from (6) and the impact force is estimated from (1) with $k = N$. It should be noted that if the relationship between the vectors $\mathbf{X}^j$ and $\mathbf{Y}^j$ is linear, then (1) gives the exact solution for $\mathbf{Y}$. In any other case, $\hat{\mathbf{Y}}$ is a linear approximation of the vector $\mathbf{Y}$. The quality of this approximation depends on the topology of the relationship between the vectors $\mathbf{X}^j$ and $\mathbf{Y}^j$, and on the distance among the neighbors vectors. Here we will study the proposed approximation using neighbors with two different distances between them, and the results will be compared with other algorithms such as ANN and LSSVM.

3. Experimental application

Figure 4 presents the experimental setup, which corresponds to an aluminum plate with dimensions 490 mm x 390 mm x 2.5 mm that is simply supported by four screws. The plate is excited by an instrumented impact hammer and the response is captured by four piezoelectric discs of 20 mm diameter and 0.42 mm thickness bonded to the surface. Data from the four sensors and impact hammer is recorded with a sampling rate of 24 kHz. The hammer is used as trigger and 1000 data points before the impact and 9000 data points after the impact are recorder.

The impact hammer has three interchangeable tips made of steel, aluminum and plastic. Figure 5 presents examples of impacts in the time and frequency domain obtained with the different tips. The main difference between impact with different hammer tips is their width and frequency content.

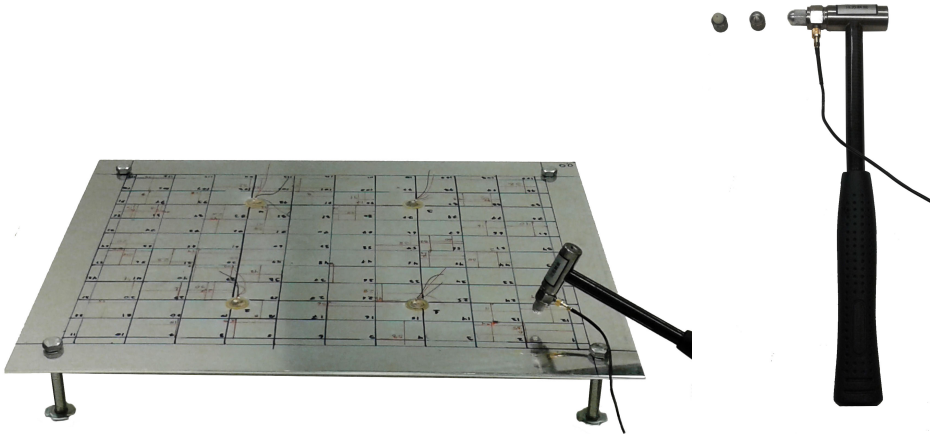

(a) Plate

(b) Impact hammer and tips

Figure 4. Experimental setup.

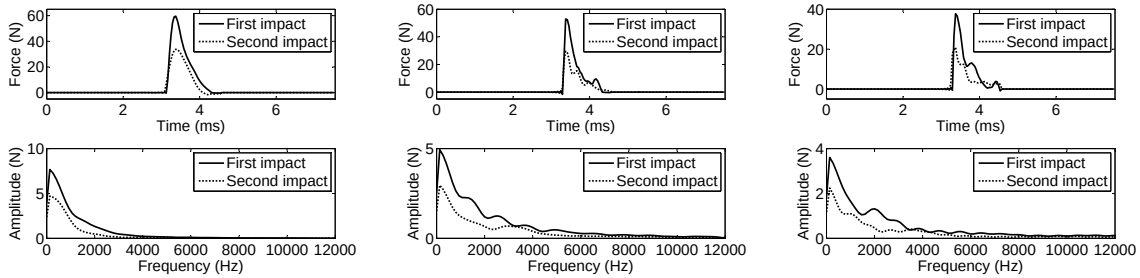

(a) Plastic tip. (b) Aluminum tip. (c) Steel tip.

Figure 5. Examples of impacts obtained with different hammer tips.

Six sets of impact data are acquired, two for training, one to set up the parameters of the identification algorithms and three to evaluate. The training sets consist of a uniform grid of 117 and 36 points respectively, as shown in Figures 6(a) and 6(b). In the first training set the spacial distance between impact point is 40 mm in the x-direction and 30 mm in the y-direction, whereas for the second training set the distance is 80 mm in the x-direction and 60 mm in the y-direction. In both cases, each point is impacted once using the plastic tip. The third set consists of 20 random impacts distributed over the plate as shown in Figure 6(c), each point is impacted once using the plastic tip. The fourth, fifth and sixth sets consist of 35 random impacts distributed over the plate as shown in Figure 6(d), each point is impacted once using the plastic, aluminum and steel tips, respectively.

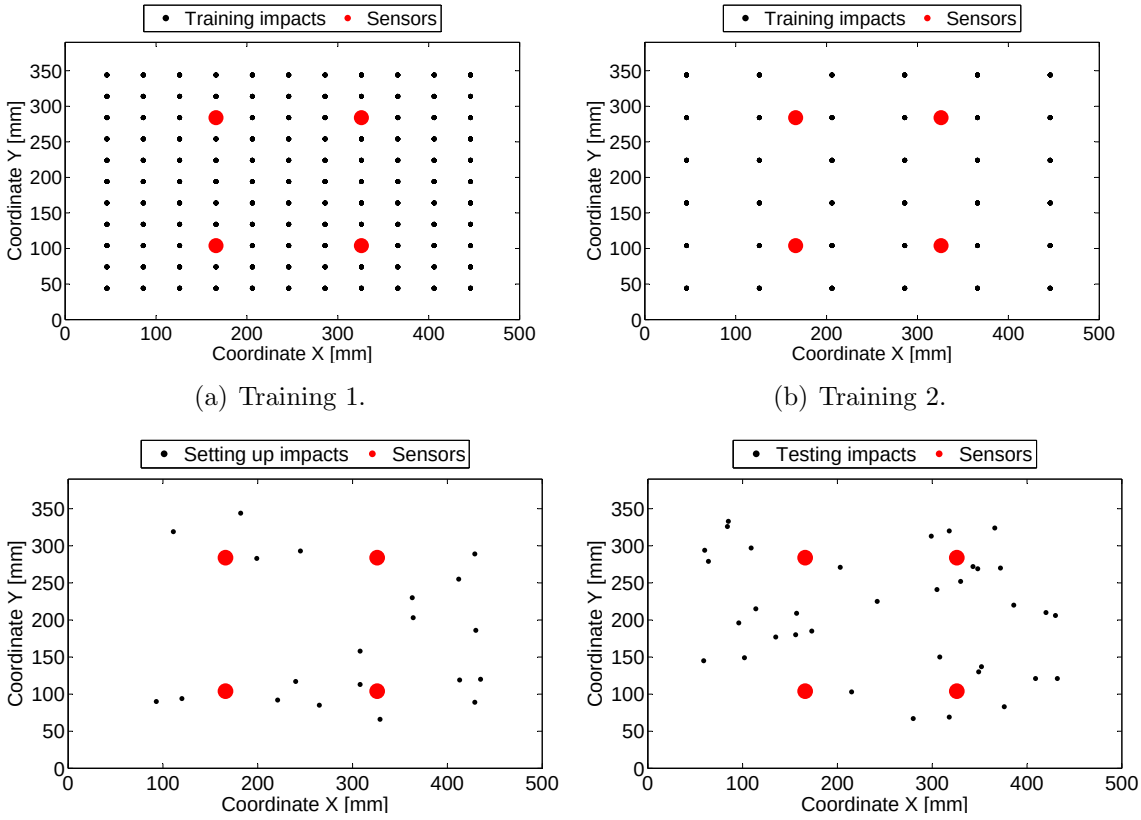

(a) Training 1. (b) Training 2.

(c) Setting up. (d) Testing.

Figure 6. Location of the experimental impacts applied to the plate.

The structure is linear, and in consequence the response is proportional to the magnitude of the force. Therefore, the response to impacts of different magnitudes can be determined by simply multiplying the measured response by scaling factors. With this methodology the initial training sets of 117 and 36 impacts are expanded to two sets of 1521 and 468 impacts with magnitudes between 5 N and 250 N.

4. Results and discussions

Three regression algorithms for impact identification have been evaluated: LME, LSSVM and ANN. To quantify the performance of the algorithms, the following error functions are defined:

$$E_x = \frac{1}{n}\sum_{j=1}^{n}\left|\hat{\mathbf{Y}}_1^j - \mathbf{Y}_1^j\right|, \tag{10}$$

$$E_y = \frac{1}{n}\sum_{j=1}^{n}\left|\hat{\mathbf{Y}}_2^j - \mathbf{Y}_2^j\right|, \tag{11}$$

$$E_F = \frac{1}{n}\sum_{j=1}^{n}\frac{\left|\hat{\mathbf{Y}}_3^j - \mathbf{Y}_3^j\right|}{\mathbf{Y}_3^j} \times 100, \tag{12}$$

$$E_A = \frac{E_x \times E_y}{A} \times 100 = \frac{\sum_{j=1}^{n} \left|\hat{\mathbf{Y}}_1^j - \mathbf{Y}_1^j\right| \sum_{j=1}^{n} \left|\hat{\mathbf{Y}}_2^j - \mathbf{Y}_2^j\right|}{n^2 A} \times 100, \qquad (13)$$

where n is the number of elements in the testing database; A is the area of the plate; E_x and E_y are the mean errors in the estimation of the force in the x and y coordinates; E_F is the percentage error in the estimation of the force magnitude, and E_A is the percentage area localization error. The results for each algorithm are presented next.

4.1. LME

The procedure to identify impacts using LME is implemented as follows:

(i) Perform an experimental impact test on the plate and construct the feature vector $\mathbf{X}$.

(ii) Read the feature vectors in the database.

(iii) Select the parameter β_i in the Gaussian prior (6), so that k neighbors contribute to the solution.

(iv) Solve the system of nonlinear equations presented in (9).

(v) Compute the weight functions from (7).

(vi) Read the observation vectors in the database and estimate the experimental impact from (1).

The only parameter that needs to be selected is the number of neighbors that contribute to the solution. To select this parameter, the algorithm performance was evaluated with different number of neighbors using the setting up database. Figures 7 and 8 present the results for E_F and E_A as a function of the number of neighbors for the two training databases. To minimize the area error while keeping a low force error, 260 neighbors were selected in both cases. Figures 9 to 11 show the impact identification results using both training databases and the three evaluation databases.

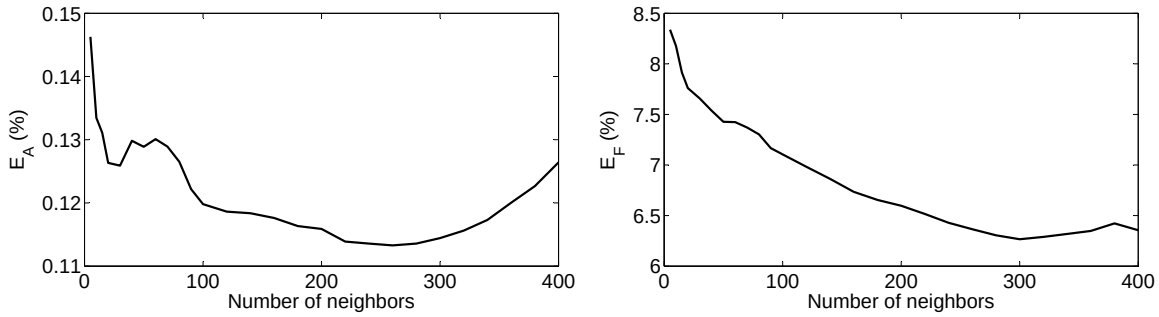

(a) Area error. (b) Force error.

Figure 7. Force and area error as a function of the number of neighbors in the LME algorithm for the first training database.

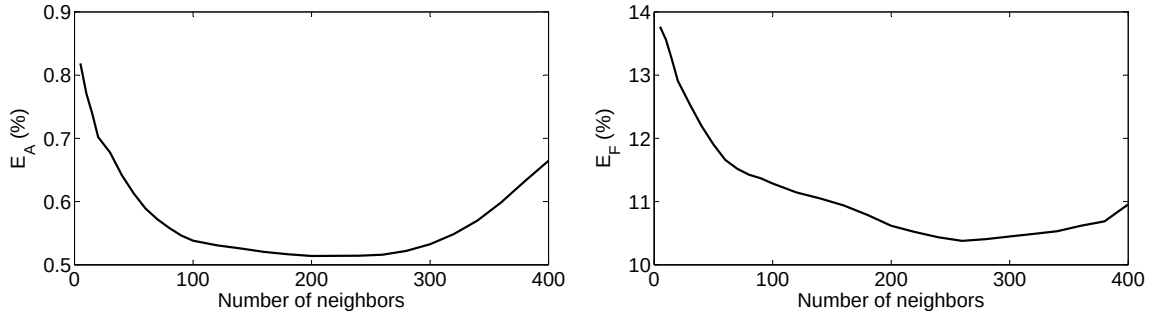

(a) Area error. (b) Force error.

Figure 8. Force and area error as a function of the number of neighbors in the LME algorithm for the second training database.

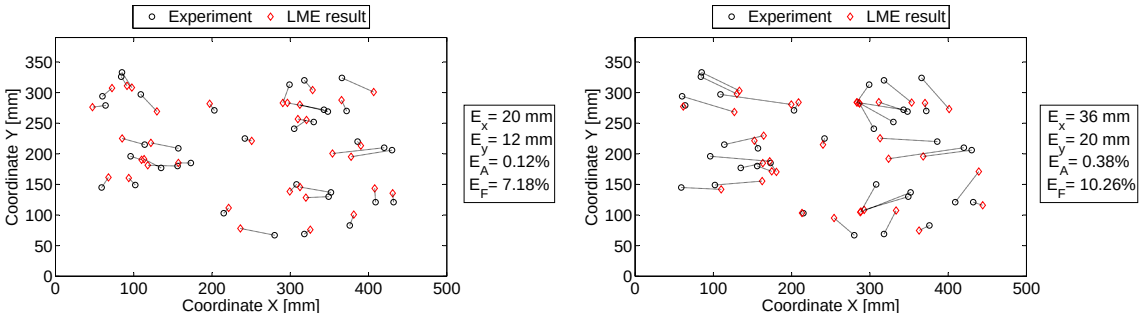

(a) Training database 1. (b) Training database 2.

Figure 9. LME results for the testing database with a plastic tip.

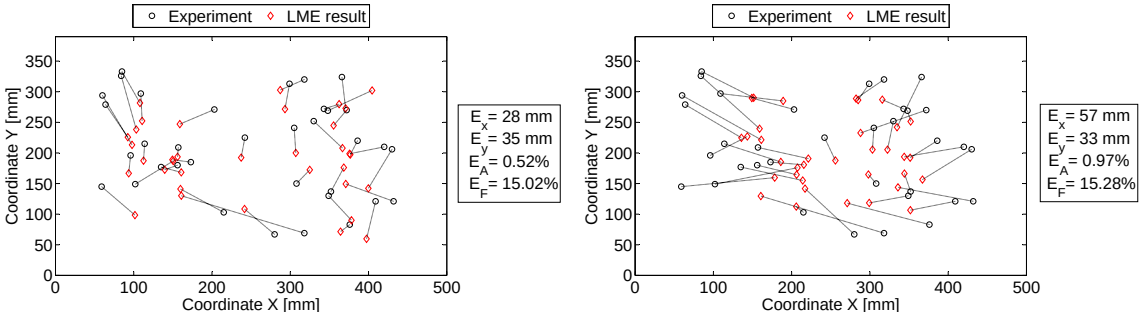

(a) Training database 1. (b) Training database 2.

Figure 10. LME results for the testing database with an aluminum tip.

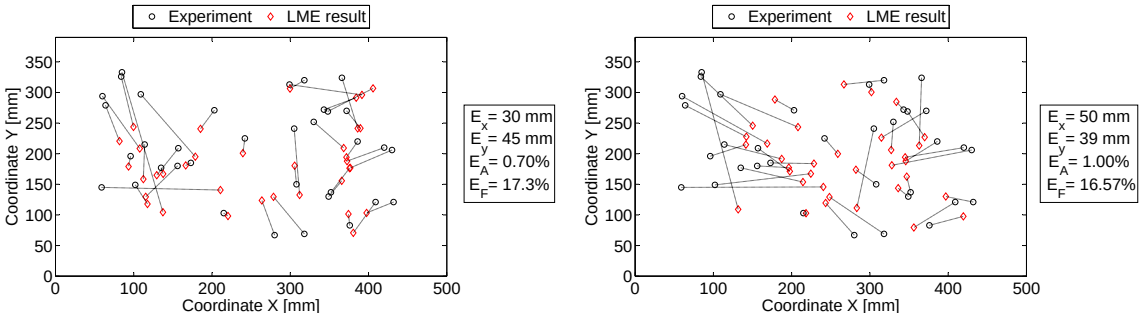

(a) Training database 1. (b) Training database 2.

Figure 11. LME results for the testing database with a steel tip.

4.2. LSSVM

The LSSVM was implemented in Matlab using the toolbox developed by Brabanter et al. [35]. Since the LSSVM is a single-output variable algorithm, three LSSVM were trained: the first to identify the force magnitude, and the second and third are trained to locate the force in the x and y coordinates. The three algorithms have twelve input parameters corresponding to the feature vector and one output. As selected in [13], the kernel function is a radial basis function (RBF).

Two parameters need to be selected, the regularization parameter, γ, and the kernel parameter, σ. To select them, the performance of the three LSSVM trained with different combinations of γ and σ were evaluated using the setting up database. The results for the area and force errors are presented in Figures 12 and 13. For the first training database, the minimum area error is obtained for $\gamma = 1.2$ and $\sigma = 3$ and the force error is minimized with $\gamma = 0.9$ and $\sigma = 15.5$. Therefore, in this case the first LSSVM algorithm uses $\gamma = 0.9$ and $\sigma = 15.5$, and the second and third LSSVM algorithms use $\gamma = 1.2$ and $\sigma = 3$.

For the second training database, the minimum area error is obtained for $\gamma = 0.3$ and $\sigma = 10.5$ and the force error is minimized with $\gamma = 0.5$ and $\sigma = 16.5$. Therefore, in this case the first LSSVM algorithm uses $\gamma = 0.5$ and $\sigma = 16.5$, and the second and third LSSVM algorithms use $\gamma = 0.3$ and $\sigma = 10.5$. Figures 14 to 16 show the impact identification results using both training databases and the three evaluation databases.

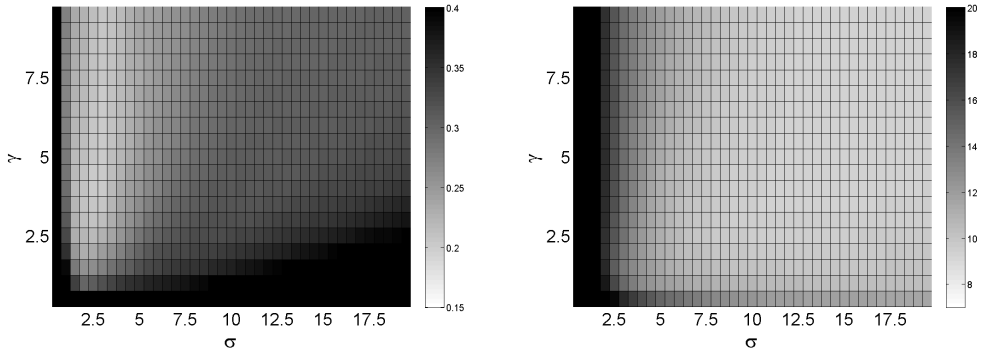

(a) Area error. (b) Force error.

Figure 12. Area and force error as a function of the parameters σ and γ in the LSSVM algorithm for the first training database.

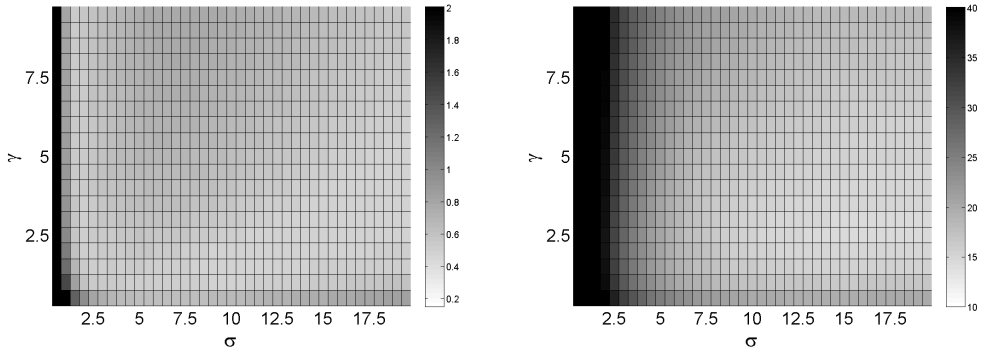

(a) Area error. (b) Force error.

Figure 13. Area and force error as a function of the parameters σ and γ in the LSSVM algorithm for the second training database.

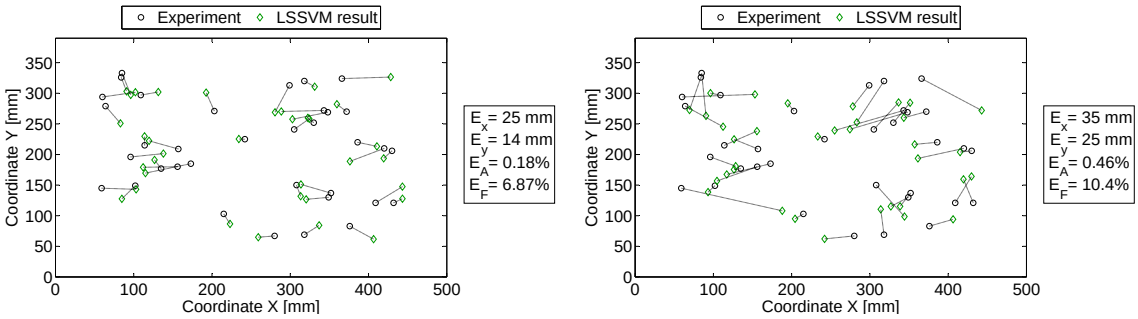

(a) Training database 1. (b) Training database 2.

Figure 14. LSSVM results for the testing database with a plastic tip.

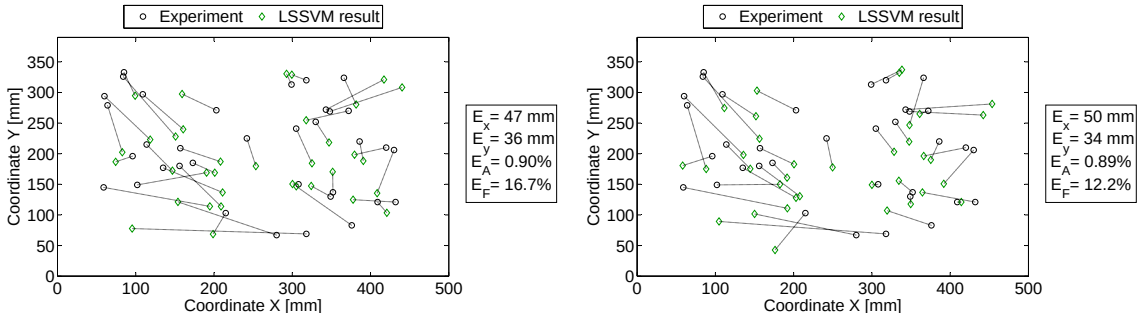

(a) Training database 1. (b) Training database 2.

Figure 15. LSSVM results for the testing database with an aluminum tip.

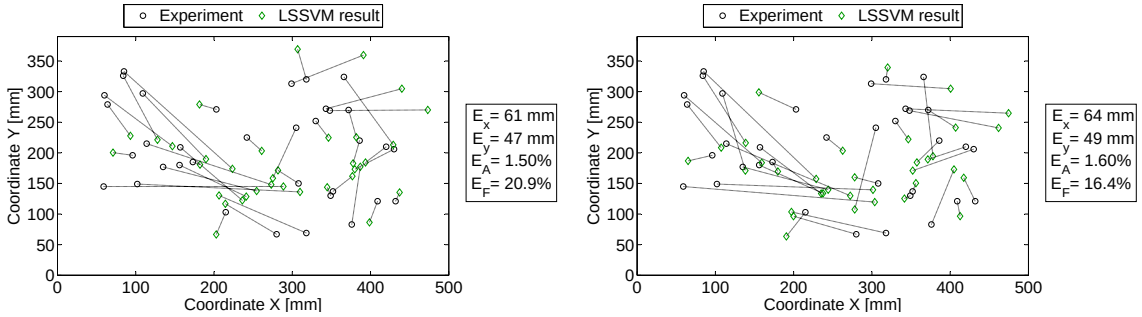

(a) Training database 1. (b) Training database 2.

Figure 16. LSSVM results for the testing database with a steel tip.

4.3. ANN

The ANN used in the current investigation has the same parameters and architecture than the one used by Xu [13]. Therefore, a three-layer ANN is trained using the Levenberg-Marquardt algorithm. The training sets are used to train the network, during training these sets are divided into two subsets of 80% for training and 20% for validating. The algorithm trains the network using the early stopping technique, this is, when the validation error increases for a number iterations, the algorithm stops the training. The weights of the network at the minimum validation error become the final weights. The transfer function in the hidden layer is *hyperbolic tangent sigmoid* and the transfer function in the output layer is *linear*.

The network has twelve input neurons corresponding to the parameters of the feature vector, and three output neurons corresponding to the force coordinates and magnitude. The number of hidden neurons is selected after a sensitivity analysis; the network is trained with different number of hidden neurons and the performance is evaluated with the setting up database. The results for both training databases are illustrated in Figures 17 and 18, the minimum force and area errors are obtained with six hidden neurons for the first training database and with three hidden neurons for the

second training database. Figures 19 to 21 show the impact identification results using both training databases and the three evaluation databases.

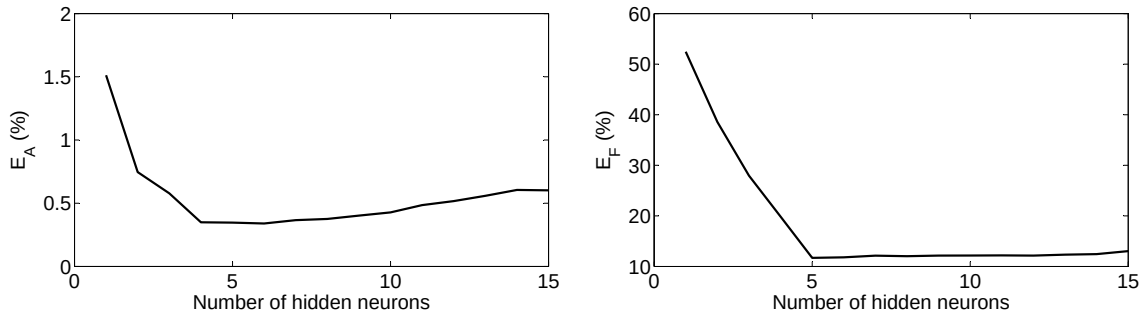

(a) Area error. (b) Force error.

Figure 17. Area and Force error as a function of the number of neighbors in the ANN algorithm for the first training database.

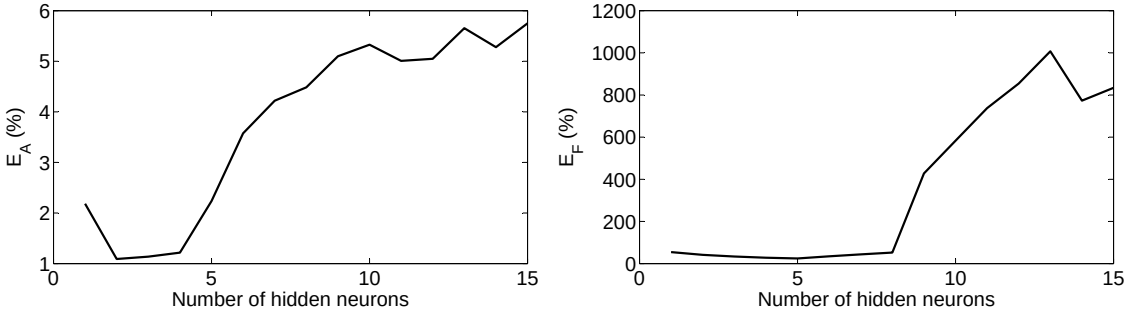

(a) Area error. (b) Force error.

Figure 18. Area and Force error as a function of the number of neighbors in the ANN algorithm for the second training database.

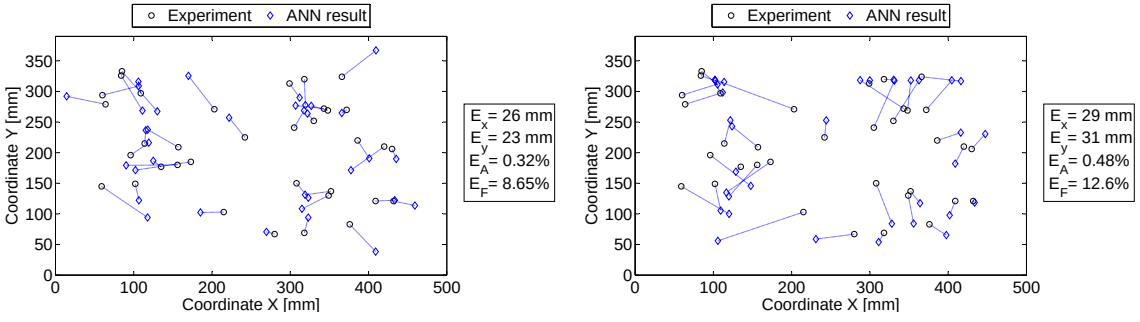

(a) Training database 1. (b) Training database 2.

Figure 19. ANN results for the testing database with a plastic tip.

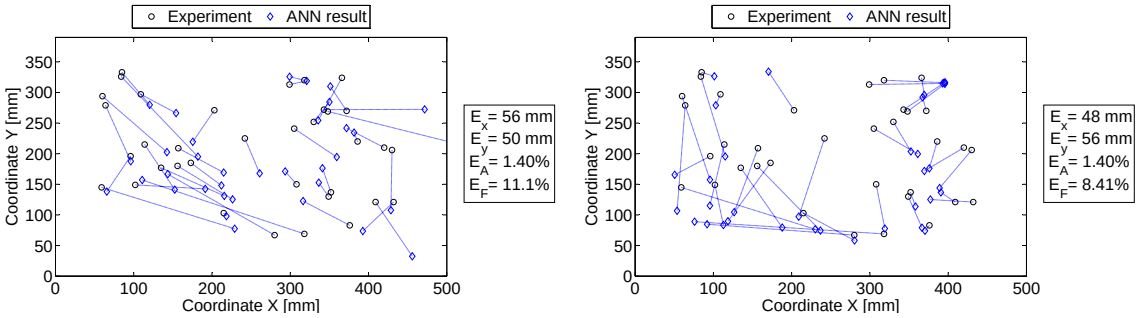

(a) Training database 1. (b) Training database 2.

Figure 20. ANN results for the testing database with an aluminum tip.

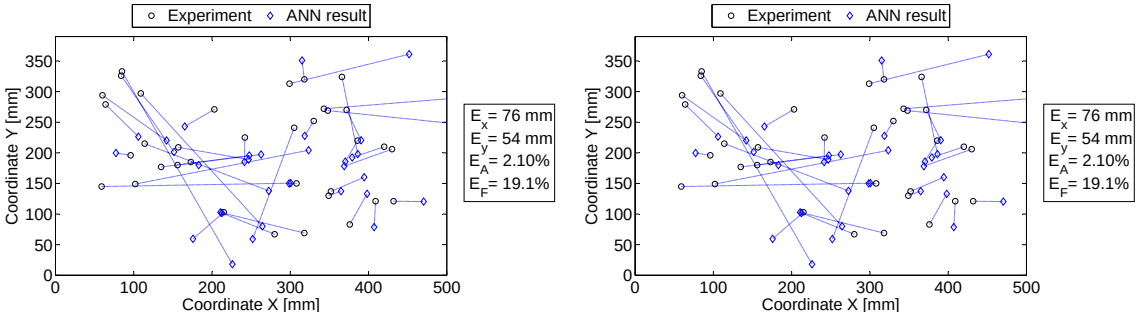

(a) Training database 1. (b) Training database 2.

Figure 21. ANN results for the testing database with a steel tip.

4.4. Discussions

Tables 1 and 2 summarize the testing results for the three evaluated algorithms.

As expected, the accuracy of the impact identification algorithms dismisses when the testing database is build with a different type of impacts (different hammer tip) than those of the training database. This is because the features selected to identify impact are affected by the frequency content of the signal, and by modifying the hammer tip the frequency content of the impact and response signals changes.

In addition, the best results are obtained when the distance between impacts in the database is smaller (training database 1). This is further studied in table 3, where the localization error (E_x and E_Y) is compared with the spatial distance between training impacts (Δx and Δy). It can be concluded that the localization error is directly related to the distance between training impacts, and that the ratio between the LME localization error and this distance is in the range 0.3-0.5 when the same hammer tip is used in the training and testing databases.

In general, the best results are obtained for the LME and LSSVM algorithms. Looking at the average results for the fist training database in table 1, the area error of LME is 48% lower than the error of LSSVM and 65% lower than the error of ANN, whereas the force error of LME is 11% lower than the error of LSSVM and 2% higher

than the error of ANN. On the other hand, for the second training database, in average, the area error of LME is 20% lower than the error of LSSVM and 55% lower than the error of ANN, whereas the force error of LME is 14% higher than the error of LSSVM and 1% lower than the error of ANN. It can be concluded that the LME algorithm provides a lower area error and that the force error is similar for the three algorithms.

Table 1. Performance of the three impact identification algorithms for the first training database.

		Identification algorithm		
Testing Database		LME	LSSVM	ANN
Plastic	Area Error (%)	0.12	0.18	0.32
	Force Error (%)	7.18	6.87	8.65
Aluminum	Area Error (%)	0.52	0.90	1.40
	Force Error (%)	15.02	16.70	11.1
Steel	Area Error (%)	0.70	1.50	2.10
	Force Error (%)	17.30	20.90	19.10
Average	Area Error (%)	0.45	0.86	1.27
	Force Error (%)	13.17	14.82	12.95

Table 2. Performance of the three impact identification algorithms for the second training database.

		Identification algorithm		
Testing Database		LME	LSSVM	ANN
Plastic	Area error (%)	0.38	0.46	0.48
	Force error (%)	10.26	10.40	12.60
Aluminum	Area error (%)	0.97	0.89	1.40
	Force error (%)	15.28	12.20	8.41
Steel	Area error (%)	1.00	1.60	3.40
	Force error (%)	16.57	16.40	14.80
Average	Area error (%)	0.78	0.98	1.76
	Force error (%)	11.85	10.42	11.94

Table 3. LME impact localization error as a function of the distance between training impacts, plastic tip.

	Δx (mm)	Δy (mm)	E_x (mm)	E_y (mm)	$E_x/\Delta x$	$E_y/\Delta y$
Training Database 1	40	30	20	12	0.50	0.40
Training Database 2	80	60	36	20	0.45	0.33

Table 4 compares the results of LME with those of other algorithms available in the literature for similar structures (composite or aluminum plates). In this case, the results

of the testing database with a plastic tip are presented, since other works in the literature use the same tip in the training and testing database. Among these algorithms, LME reaches the lowest combination of force and area error. The work of Fu and Xu [9] has a similar area error with the same number of sensor and less training impact points and the time-reversal algorithm [18] has a lower area error under the same circumstances. However, these methods can only locate an impact and does not quantify it. It should be noted that to assess possible damage in the structure, it is important to estimate the magnitude of the impact. In this context, the proposed methodology is more accurate than other algorithms available, with a force error 64% lower than that of the best algorithm in Table 2.

Table 4. Comparison between impact identification algorithms available in the literature and current work.

Reference	Algorithm	Plate size (mm^2)	Number of sensors	Number of training impact points	Area error (%)	Force error (%)
Worden and Staszewski [3]	ANN	530x300	17	80	0.37	20.1
Haywood et al. [5]	ANN	608x304	12	63	0.21	-
Xu [13]	LSSVM	490x390	4	63	1.06	51.2
Fu and Xu [9]	PCA+SVM	490x390	4	63	0.13	-
Xu [12]	Kernel-ELM	490x390	4	63	0.74	-
Fu et al. [11]	PCA+Kernel-ELM	490x390	4	63	0.24	-
Ing et al. [18]*	Time-reversal	490x390	4	117	0.08	-
Current work	LME	490x390	4	117	0.12	7.18
Current work	LME	490x390	4	36	0.38	10.26

* The results of the time-reversal algorithm have been computed with our experimental data following the procedure proposed by Ing et al. [18].

5. Conclusions

This article presented a new regression algorithm for impact identification that uses a linear approximation handled by a statistical inference model based on the maximum-entropy principle, termed linear approximation with maximum entropy (LME). The performance of the proposed methodology was validated by considering an experimental aluminum plate. Time varying strain data was measured using four piezoceramic sensors bonded to the plate.

To demonstrate the potential of the proposed approach over existing ones, results obtained via LME were compared with those of Artificial Neural Networks (ANN) and Least Square Support Vector Machines (LSSVM). In terms of force localization (area

error), the best performance is obtained with LME followed by LSSVM and last is ANN. Regarding force quantification, the results of the three algorithms are similar.

The comparison with other impact identification algorithms available in literature shows that the impact localization can be improved by using the time-reversal approach. A subject of future research is to create a hybrid approach that combines times reversal with LME.

Although the structure under investigation was a simple metallic plate, the results demonstrated that with a low number of sensors it is possible to accurately locate and quantify impacts and that LME outperforms others impact identification algorithms. Nonetheless, it is necessary to study the performance in composite materials and in structures with more complex geometries than a plate.

References

[1] R. Seydel and F.-K. Chang. Impact identification of stiffened composite panels: I. system development. *Smart Materials and Structures*, 10(2):354–369, 2001.

[2] R. Seydel and F.-K. Chang. Impact identification of stiffened composite panels: Ii. implementation studies. *Smart Materials and Structures*, 10(2):370–379, 2001.

[3] K. Worden and W.J. Staszewski. Impact location and quantification on a composite panel using neural networks and a genetic algorithm. *Strain*, 36(2):61–68, 2000.

[4] P.T. Coverley and W.J. Staszewski. Impact damage location in composite structures using optimized sensor triangulation procedure. *Smart materials and structures*, 12(5):795–803, 2003.

[5] J. Haywood, P.T. Coverley, W.J. Staszewski, and K. Worden. An automatic impact monitor for a composite panel employing smart sensor technology. *Smart Materials and Structures*, 14(1):265–271, 2005.

[6] J.R. LeClerc, K. Worden, W.J. Staszewski, and J. Haywood. Impact detection in an aircraft composite panela neural-network approach. *Journal of Sound and Vibration*, 299(3):672–682, 2007.

[7] L.E. Mujica, J. Vehi, W.J. Staszewski, and K. Worden. Impact damage detection in aircraft composites using knowledge-based reasoning. *Structural Health Monitoring*, 7(3):215–230, 2008.

[8] Z. Sharif-Khodaei, M. Ghajari, and M.H. Aliabadi. Determination of impact location on composite stiffened panels. *Smart Materials and Structures*, 21(10):105026, 2012.

[9] H. Fu and Q. Xu. Locating impact on structural plate using principal component analysis and support vector machines. *Mathematical Problems in Engineering*, 2013:352149, 2013.

[10] M. Ruiz, L.E. Mujica, X. Berjaga, and J. Rodellar. Partial least square/projection to latent structures (pls) regression to estimate impact localization in structures. *Smart Materials and Structures*, 22(2):025028, 2013.

[11] H. Fu, C.-M. Vong, P.-K. Wong, and Z. Yang. Fast detection of impact location using kernel extreme learning machine. *Neural Computing and Applications*, pages 1–10, 2014.

[12] Q. Xu. A comparison study of extreme learning machine and least squares support vector machine for structural impact localization. *Mathematical Problems in Engineering*, 2014:906732, 2014.

[13] Q. Xu. Impact detection and location for a plate structure using least squares support vector machines. *Structural Health Monitoring*, 31(1):5–18, 2014.

[14] W.J. Staszewski, K. Worden, R. Wardle, and G.R. Tomlinson. Fail-safe sensor distributions for impact detection in composite materials. *Smart Materials and Structures*, 9(3):298–303, 2000.

[15] T. Van Gestel, J.A.K. Suykens, B. Baesens, S. Viaene, J. Vanthienen, G. Dedene, B. De Moor, and J. Vandewalle. Benchmarking least squares support vector machine classifiers. *Machine Learning*, 54(1):5–32, 2004.

[16] G.-B. Huang, Q.-Y. Zhu, and C.-K Siew. Extreme learning machine: a new learning scheme of feedforward neural networks. In *IEEE International Joint Conference on Neural Networks*, volume 2, pages 985–990. IEEE, 2004.

[17] G.-B. Huang, D.H. Wang, and Y. Lan. Extreme learning machines: a survey. *International Journal of Machine Learning and Cybernetics*, 2(2):107–122, 2011.

[18] Ros Kiri Ing, Nicolas Quieffin, Stefan Catheline, and Mathias Fink. In solid localization of finger impacts using acoustic time-reversal process. *Applied Physics Letters*, 87(20):204104, 2005.

[19] Guillemette Ribay, Stefan Catheline, Dominique Clorennec, R Kiri Ing, Nicolas Quieffin, and Mathias Fink. Acoustic impact localization in plates: properties and stability to temperature variation. *IEEE transactions on ultrasonics, ferroelectrics, and frequency control*, 54(2):378–385, 2007.

[20] Byeongjin Park, Hoon Sohn, Steven E Olson, Martin P DeSimio, Kevin S Brown, and Mark M Derriso. Impact localization in complex structures using laser-based time reversal. *Structural Health Monitoring*, 11(5):577–588, 2012.

[21] Francesco Ciampa and Michele Meo. Impact detection in anisotropic materials using a time reversal approach. *Structural Health Monitoring*, 11(1):43–49, 2012.

[22] M.R. Gupta. *An information theory approach to supervised learning*. PhD thesis, Stanford University, 2003.

[23] M.R. Gupta, R.M. Gray, R. Olshen, et al. Nonparametric supervised learning by linear interpolation with maximum entropy. *IEEE Transactions on Pattern Analysis and Machine Intelligence,*, 28(5):766–781, 2006.

[24] E.T. Jaynes. Information theory and statistical mechanics. *Physical Review*, 106(4):620–630, 1957.

[25] V. Meruane, V. Del Fierro, and A. Ortiz-Bernardin. A maximum entropy approach to assess debonding in honeycomb aluminum plates. *Entropy*, 16(5):2869–2889, 2014.

[26] V. Meruane and A. Ortiz-Bernardin. Structural damage assessment using linear approximation with maximum entropy and transmissibility data. *Mechanical Systems and Signal Processing*, 54:210–223, 2015.

[27] T.J. Ulrich. Envelope calculation from the hilbert transform. Technical report, Los Alamos National Laboratory, 2006.

[28] Luc Devroye, Laszlo Gyorfi, Adam Krzyzak, and Gabor Lugosi. On the strong universal consistency of nearest neighbor regression function estimates. *The Annals of Statistics*, pages 1371–1385, 1994.

[29] Riccardo Rovatti, Michele Borgatti, and Roberto Guerrieri. A geometric approach to maximum-speed n-dimensional continuous linear interpolation in rectangular grids. *IEEE Transactions on Computers*, 47(8):894–899, 1998.

[30] C.E. Shannon. A mathematical theory of communication. *The Bell Systems Technical Journal*, 27:379–423, 1948.

[31] N. Sukumar and R.W. Wright. Overview and construction of meshfree basis functions: from moving least squares to entropy approximants. *International Journal for Numerical Methods in Engineering*, 70(2):181–205, 2007.

[32] S. Kullback. *Information Theory and Statistics*. Wiley, New York, NY, 1959.

[33] J.E. Shore and R.W. Johnson. Axiomatic derivation of the principle of maximum entropy and the principle of minimum cross-entropy. *IEEE Transactions on Information Theory*, 26(1):26–36, 1980.

[34] M. Arroyo and M. Ortiz. Local maximum-entropy approximation schemes: a seamless bridge between finite elements and meshfree methods. *International Journal for Numerical Methods in Engineering*, 65(13):2167–2202, 2006.

[35] K. De Brabanter, P. Karsmakers, F. Ojeda, C. Alzate, J. De Brabanter, K. Pelckmans, B. De Moor, J. Vandewalle, and J.A.K. Suykens. Ls-svmlab toolbox users guide. *ESAT-SISTA Technical Report*, pages 10–146, 2011.